Focusing Bistatic SAR Images using Non-Linear Chirp Scaling

Y.L. Neo, F. H. Wong, I. Cumming

University of British Columbia

Abstract: Non-Linear Chirp Scaling is an innovative way to focus bistatic SAR images and has been demonstrated to work on the configuration where the transmitter imaging on broadside and the receiver is stationary. This paper improves and extends the method to the configuration where both the receiver and the transmitter are imaging at a squint angle and moving in a parallel track with the same velocity. Simulated point targets using flight configurations similar to the airborne ONERA/DLR bistatic SAR experiments are used to verify the focusing algorithm.

Keywords: Bistatic SAR processing, Non-Linear Chirp Scaling, parallel tracks.

1. Introduction

Traditional monostatic algorithms, such as the Range Doppler and Chirp Scaling algorithms, may not work well in a bistatic environment. A review of existing bistatic SAR algorithms such as the wavenumber algorithm [1] and the Back Projection Algorithm [2] was conducted and it was concluded that Non-Linear Chirp Scaling (NLCS) algorithm [3] could be a useful alternative. This paper extends and improves the existing Non-Linear Chirp Scaling algorithm to focus a bistatic image where both platforms are moving in a parallel track with the same velocity.

A joint X-band bistatic SAR experiment by ONERA/DLR [4] was carried out to explore the challenges associated with bistatic radar. It involves the use of two separate monostatic SAR systems carried by E-SAR and RAMSES, imaging at broadside. Two separate configurations were used in their experiments, both involving parallel flight paths and low squint angles. The algorithm developed in this paper can be used to focus both cases.

2. Bistatic SAR Imaging Model

Bistatic SAR has separate transmitter and receiver sites, whereby each platform can assume different velocities and different flight paths, as shown in Fig. 1. Together with the target, these three sites form the vertices of the bistatic triangle that lies in the bistatic imaging plane. The angle between the line of sight of the transmitter and the line of sight of the receiver forms the bistatic angle β. The baseline is the line joining the transmitter and the receiver.

In the configurations considered, the transmitter works in stripmap mode while the receiver steers its antenna footprint to match the transmitter antenna footprint. In some configurations, the baseline and the bistatic angle change with time.

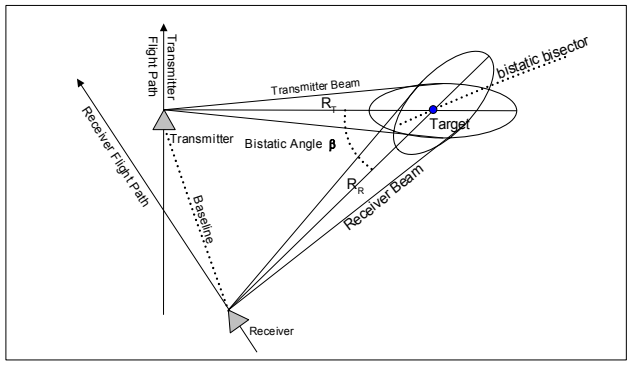

Figure 1 : Imaging Geometry of Bistatic SAR

3. Non-Linear Chirp Scaling Algorithm

3.1 The Existing NLCS Algorithm

Fig. 2 illustrates the main steps taken in the NLCS Algorithm [3]. The first step of the algorithm is range compression. After range compression, Range Cell Migration (RCM) of target trajectories can be observed. In most cases, the dominant term of the RCM is the linear component. The quadratic and higher component is usually small, especially for short wavelength systems.

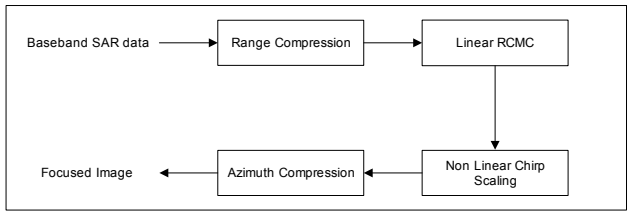

Figure 2 : Existing NLCS Algorithm

Linear RCM correction (LRCMC) using linear interpolation is applied after range compression. The Linear RCMC step eliminates most of the RCM and the range/azimuth phase coupling, which facilitates the processing of high squint cases. After LRCMC, targets with different FM rates (since they have different ranges of closest approach) fall into the same range gate. NLCS is applied to equalize the FM rates along each range cell by using a perturbation function. Once the azimuth FM

rate is equalized for all range gates, the image can be focused by conventional means.

3.2 Extending the NLCS Algorithm

In the existing NLCS algorithm [3], simulated point target experiments were documented for a monostatic case and simple bistatic cases where the receiver is stationary and the transmitter antenna pointing at zero Doppler. We have extended the algorithm to include parallel flight cases with a modified perturbation function in the chirp scaling step. Range focusing has also been improved by incorporating a QRCM correction step in the NLCS processing, as shown in Fig. 3.

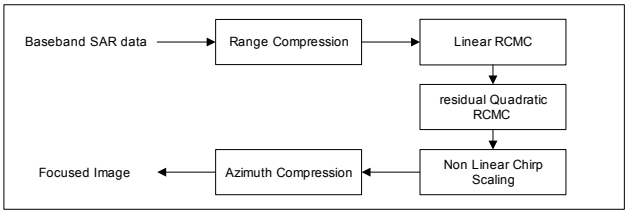

Figure 3 : Extended NLCS Algorithm

3.3 NLCS on a Parallel Tracks, Same Velocity Case

In this configuration, both the transmitter and receiver are flying in a parallel flight path, with both antennae pointing at constant squint angles. Fig. 4 shows a typical flight configuration.

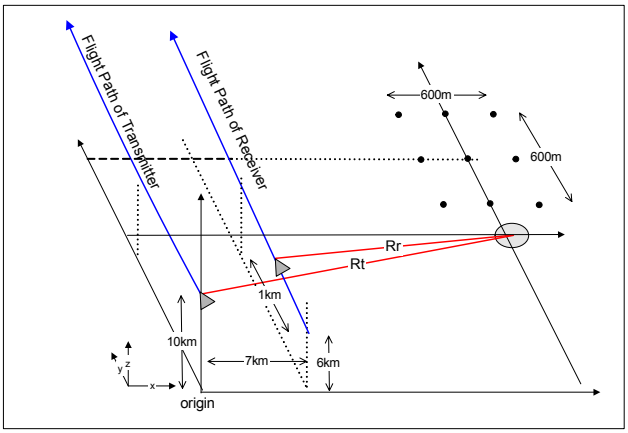

Figure 4 : Flight geometry of simulated parallel track same velocity case

The instantaneous slant range of this bistatic configuration is given by

$$R(\eta) = R_T(\eta) + R_R(\eta) \qquad [1]$$

where η is the azimuth time, R_T is the slant range to the target at the time it is illuminated by the transmitter beam centre, R_R is the slant range from the target to the receiver at the same time. These slant ranges can be written as

$$R_T(\eta) = \sqrt{R_{to}^{\,2} + V_T^{\,2}(\eta)^2} \qquad [2]$$

and

$$R_R(\eta) = \sqrt{R_{ro}^{\,2} + V_R^{\,2}(\eta - \eta_o)^2} \qquad [3]$$

where R_{to} is the slant range of closest approach of the transmitter which occurs at mid azimuth time $\eta = 0$ and R_{ro} is the slant range of closest approach of the receiver which occurs at azimuth time $\eta = \eta_o$. V_T is the transmitter velocity and V_R is the receiver velocity.

The Linear FM rate K_a of a point target is given by

$$K_a = \frac{1}{\lambda}\frac{d^2}{d\eta^2}(R_T(\eta) + R_R(\eta))$$
$$= \frac{V_T^{\,2}\cos^2\theta_{sqT}}{\lambda R_T^{\,2}} + \frac{V_R^{\,2}\cos^2\theta_{sqR}}{\lambda R_R^{\,2}} \qquad [4]$$

Both the squint angle of the receiver θ_{sqR} and squint angle of transmitter θ_{sqT} are constants in this case.

A simple flight geometry is shown in Fig. 5 with three point targets A, B and C. Point B and Point C have the same range from the flight paths. The time delay of the beam crossing of point C from that of point B is η_d. Point A and Point B have the same beam crossing time. For processing purposes, point A is chosen as the reference point.

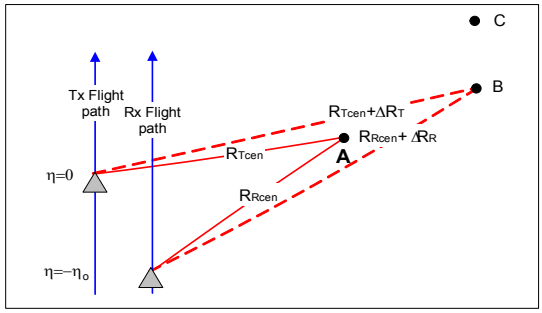

Figure 5 : Targets in a flight geometry

The target trajectories of the three point targets before and after linear RCMC are shown in Fig. 6.

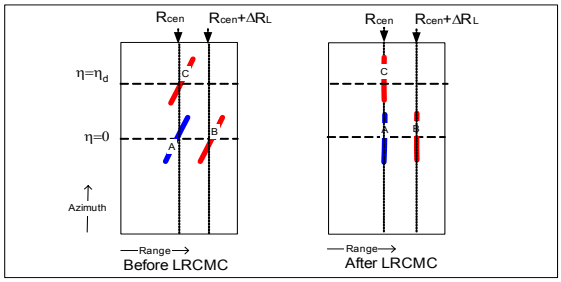

Figure 6 : Trajectories of targets

The azimuth FM rate of point A is given by

$$K_{a,0} = \frac{V_T^{\,2}\cos^2\theta_{sqT}}{\lambda R_{Tcen}^{\,2}} + \frac{V_R^{\,2}\cos^2\theta_{sqR}}{\lambda R_{Rcen}^{\,2}} \quad [5]$$

where R_{Tcen} gives the transmitter range to point A at mid azimuth time and R_{Rcen} gives the receiver range to point A at mid azimuth time.

Point C and Point B have the same FM rate as they have the same range equations. The FM rate is

$$K_{b,0} = \frac{V_T^{\,2}\cos^2\theta_{sqT}}{\lambda(R_{Tcen}+\Delta R_R)^2} + \frac{V_R^{\,2}\cos^2\theta_{sqR}}{\lambda(R_{Rcen}+\Delta R_T)^2} \quad [6]$$

ΔR_T and ΔR_T are the changes in the slant range components between point A and point B (see Fig. 5) and from the geometry we can approximated them as

$$\Delta R_T = \frac{R_{Tcen}}{R_{cen}}(V_R\sin\theta_{sqR} + V_T\sin\theta_{sqT})\eta_d \quad [7]$$

and

$$\Delta R_R = \frac{R_{Rcen}}{R_{cen}}(V_R\sin\theta_{sqR} + V_T\sin\theta_{sqT})\eta_d \quad [8]$$

The sum of ΔR_T and ΔR_R gives the linear RCM,

$$\Delta R_L = (V_T\sin\theta_{sqT} + V_R\sin\theta_{sqR})\eta_d \quad [9]$$

Linear RCMC is performed using the slope taken from the reference point. Linear RCMC is performed with reference to the reference point with the zero shift set to the mid azimuth line.

For a point target C, which is situated at η_d away from the mid azimuth sample, it undergoes a linear RCM of ΔR_L. After LRCMC, the trajectory of point C moves into the same range gate as point A. Fig. 6 illustrates the trajectories of point A and point C before and after LRCMC. Thus, point A and point C now lie in the same range gate although they have different FM rates. NLCS can be performed with a perturbation function to equalize the FM rates along the range gates. To find this perturbation function, we choose point target C, which is furthest away from mid azimuth sample A. The difference in the FM rates between target A and target C is given by

$$\Delta K_{a,L} = -\left(\frac{V_T^{\,2}\cos^2\theta_{sqT}K_T}{\lambda R_T^{\,2}} + \frac{V_R^{\,2}\cos^2\theta_{sqR}K_R}{\lambda R_R^{\,2}}\right)\eta_d \quad [10]$$

where K_T and K_R are proportional to the LRCM contribution by the transmitter and receiver respectively

$$K_T = \frac{R_{Tcen}}{R_{cen}}(V_R\sin\theta_{sqR} + V_T\sin\theta_{sqT}) \quad [11]$$

and

$$K_R = \frac{R_{Rcen}}{R_{cen}}(V_R\sin\theta_{sqR} + V_T\sin\theta_{sqT}) \quad [12]$$

Following the outline in [3], the perturbation function h_{pert} is found to be a cubic function of azimuth time,

$$h_{pert}(\eta) = \exp(j\pi\alpha\eta^3) \quad [13]$$

where the cubic phase coefficient is

$$\alpha = \frac{V_T^{\,2}\cos^2\theta_{sqT}K_T}{3\lambda R_T^{\,2}} + \frac{V_R^{\,2}\cos^2\theta_{sqR}K_R}{3\lambda R_R^{\,2}} \quad [14]$$

3.4 Residual QRCM

In the existing algorithm, the quadratic component of the RCM is left uncorrected, causing significant IRW broadening when residual QRCM is greater than 1 range cell. A quadratic range cell migration correction has been added (see Fig. 3) to address this limitation. By correcting the QRCM, the image focusing can be extended to higher resolution images and systems with longer wavelengths such as S-band and C-band systems.

4. Simulation Results for Bistatic Cases

Simulations were carried out to check the performance of the NLCS focusing algorithm. The first example is that of parallel tracks with same velocity, focused using the new perturbation function. Simulations were also done using ONERA/DLR parameters and configurations. The last example compares the performance of stationary receiver case mentioned in [3] and [5] with and without QRCM correction.

4.1 Flight configuration similar to the ONERA case

The ONERA configuration is shown in Fig. 7. The planes are flying in a parallel track configuration with a lateral distance of about 2.9 km. This configuration is similar to the configuration shown in Fig. 4. Simulation results show that the algorithm developed here can be used for the ONERA configuration.

In the ONERA configuration, the transmitter and receiver are pointing at broadside, therefore the RCM and range/azimuth phase coupling is small. Such a configuration can be easily focused using the NLCS. Thus, a more stringent case is used here to check the performance of the algorithm where both the transmitter and receiver are squinted.

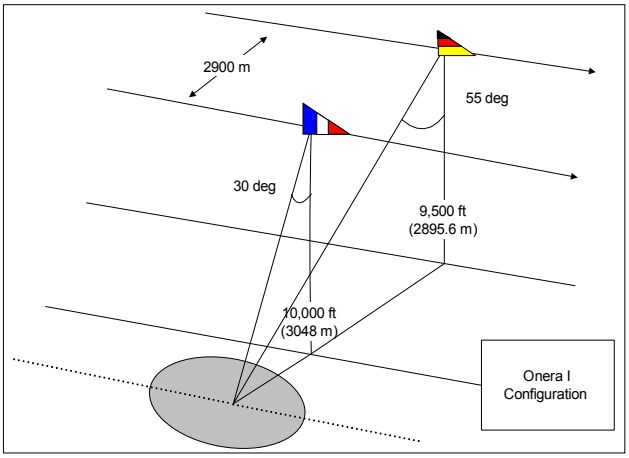

Figure 7: Simulated ONERA configuration

The simulation experiment is conducted on the point targets imaged at C-band with a transmitter squint of 25° and receiver squint of 37°. The transmitter is at an altitude of 10 km and the receiver is at an altitude of 6 km. The transmitter and receiver are laterally separated by 7 km and the receiver is slightly forward at 1 km. Both platforms fly at 200 m/sec. Bistatic angle is 13°. Nine point targets are arranged in a square grid with 600 m separation as shown in Fig. 4.

The IRW of the focused image has an error of less than 3 percent, the PSLR has an error of less than 1 dB and ISLR has an error of 1.2 dB when compared with the theoretical values. With QRCM left uncorrected, the IRW degrades by between 5 to 30 percent while PSLR has an error greater than 5.4 dB and ISLR has an error of greater than 2.1 dB from the theoretical values. Thus, the new method has a much better focusing ability.

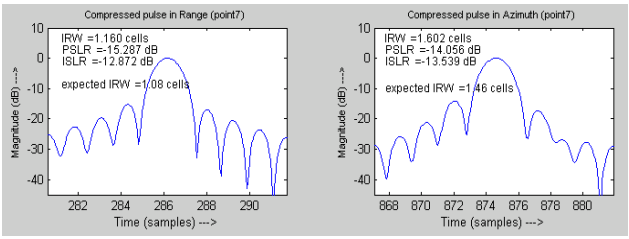

Fig. 8a. Impulse response without residual QRCMC

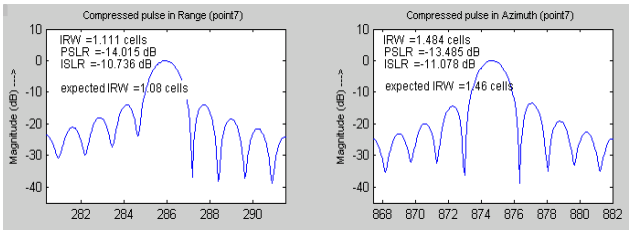

Fig. 8b. Impulse response with residual QRCMC

A typical point target response is taken from the image to illustrate the effect of using QRCMC step. The target selected (see Fig. 8) has a QRCM of 1.66 samples. Without applying residual QRCM, there is a broadening of 7.4% in the range impulse response and broadening of 9.7% in the azimuth impulse response. With residual QRCM applied, the broadening in range is reduced to 2.8% and the azimuth broadening is reduced to 1.6%.

4.2 Flight configuration similar to the DLR case

The DLR configuration is shown in Figure 9; both planes are flying along the same track in a typical "refuelling formation".

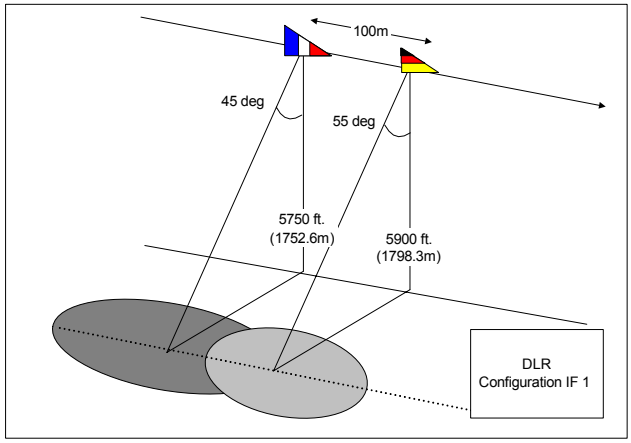

Figure 9 : simulated DLR configuration

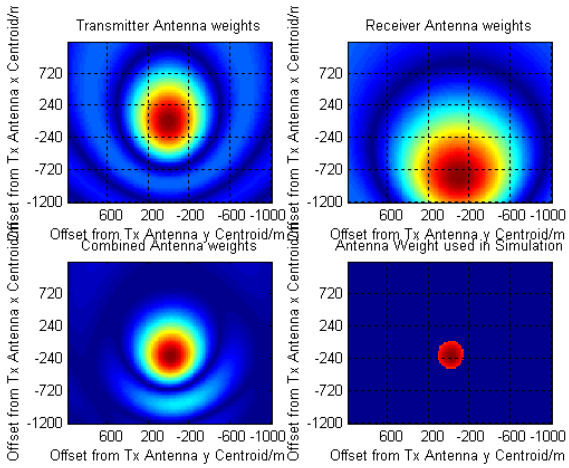

Figure 10 : Composite Antenna Footprint

A composite (round-trip) antenna pattern that has to be simulated in order to estimate the effective squint angles of the configuration correctly, since the centre of each antenna beam is pointing at different locations at a given time. Squint angles are measured to the centre of the composite beam, these angles are necessary for the LRCM correction and for Doppler centroid estimation. Using the composite antenna pattern simulated, the average squint angle for the transmitter is estimated to be -0.46° while the receiver squint angle is 1.48°. Without using the composite antenna, the transmitter squint and receiver squint would be recorded at zero squint. As shown in Table 1, the impulse response using the corrected squint angle shows a slightly better response when the composite antenna pattern is used. The error will be more pronounced if the separation between the two platforms was larger.

Table 1: Typical impulse response for simulated DLR data

Parameter	Rg IRW	Az IRW	Az PSLR	Az ISLR
Theoretical	1.237	1.015	-14.8	-11.4
with Comp.	1.237	1.003	-12.72	-10.9
w/o Comp.	1.236	1.068	-12.36	-10.5

4.3 Stationary Receiver Bistatic Case

In this configuration, the transmitter is moving in a straight line imaging at broadside while the receiver remains in a fixed position. This geometry is useful for bistatic systems where transmitters are located at on a satellite or airborne platform and receivers are located at high buildings or on top of a hill [5].

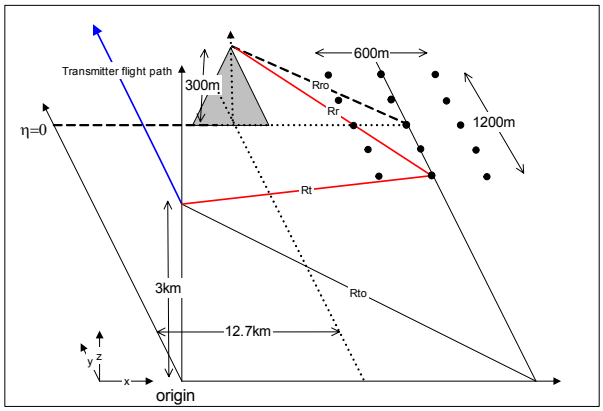

Figure 11 : Flight geometry of stationary receiver case

A simulation experiment is conducted on the point targets imaged at C-band with the transmitter imaging at broadside at an altitude of 3 km and receiver on top of a 300m hill. The transmitter and the receiver are laterally separated by 12.7 km at the closest range. The transmitter is imaging 15 point targets arranged in a grid as shown in Fig. 11.

The IRW of the focused image has an error of less than 2 percent, the PSLR has an error of less than 2 dB and ISLR has an error of 2.1 dB when compared with the theoretical values. With QRCM left uncorrected, the IRW degrades by between 5 to 25 percent while PSLR has an error greater than 4.3 dB and ISLR has an error of greater than 3.1 dB from the theoretical values. Thus, the new method has a much better focusing ability for this case as well.

The bistatic image formed is affected by the geometry of the processed data. For the stationary receiver case, point targets that lies parallel to the flight path are focused into a hyperbola, see Fig. 12a. Interpolation is required to remove this hyperbolic dependence and register the image properly as shown in Fig 12b.

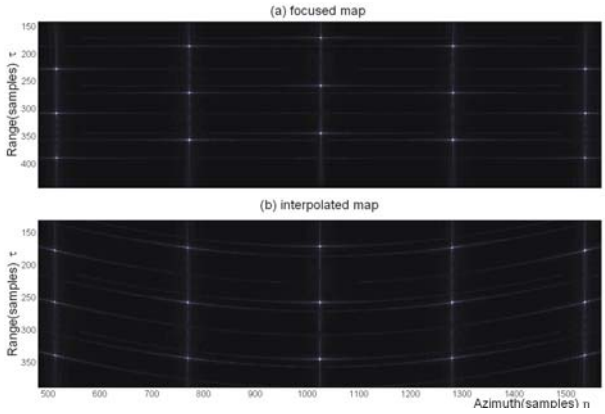

Figure 12 : Focused image of stationary receiver case

5. Conclusions

Bistatic SAR has a number of complex geometries that makes the derivation of range equation difficult. We have analyzed some of the configurations and found the NLCS to be a efficient algorithm. By deriving the range equation and the perturbation function for the parallel track, same velocity configuration, we were able to focus the bistatic data. Applying residual QRCMC further improves the impulse response for this configuration.

6. References

[1] M. Soumekh, "*Bistatic synthetic aperture radar inversion with application in dynamic object imaging*," in IEEE Trans. on Signal Processing, vol. 39, pp.2044-2055, Sep 1991.

[2] Y. Ding, D. C. Munson Jr., "*Fast Back Projection Algorithm for Bistatic SAR Imaging*," IEEE ICIP, vol II, pp 449-452. Sep 2002.

[3] F. H. Wong, and T. S. Yeo, "*New Applications of Nonlinear Chirp Scaling in SAR Data Processing*," in IEEE Trans. Geosci. Remote Sensing, vol. 39, pp. 946-953, May 2001.

[4] P. Dubois-Fernandez, et al., "*ONERA-DLR Bistatic SAR Experiment: Design of the Experiment and Preliminary Results*," in Proc. Advanced SAR Workshop, ASAR'03, Canadian Space Agency, Montreal, June 26-28, 2003..

[5] J. Sanz-Marcos, J. Mallorqui, "A bistatic SAR simulator and processor," in Proc. EUSAR 2004, Ulm, Germany, May 25-27, pp 585-588.

7. Glossary

IRW: Impulse Response Width

ISLR: Integrated Sidelobe Ratio

LRCM: Linear Range Cell Migration

NLCS: Non-Linear Chirp Scaling

PSLR: Peak Sidelobe Ratio

QRCM: Quadratic Range Cell Migration

SAR: Synthetic Aperture Radar